Nuclei function as wedges to pry open spaces and promote collective, confined cell migration *in vivo*

Lauren Penfield[a] and Denise J. Montell[a,b]

[a] Department of Molecular, Cellular, and Developmental Biology at University of California, Santa Barbara
[b] Correspondence: dmontell@ucsb.edu, Department of Molecular, Cellular, and Developmental Biology
University of California, Santa Barbara CA 93106

Abstract

Cells migrate collectively through confined environments during development and cancer metastasis. The nucleus, a stiff organelle, impedes single cells from squeezing into narrow spaces in artificial environments, but how nuclei affect collective cell migration into tissues *in vivo* is unknown. Here, we use the border cells in the fly ovary to study nuclear dynamics in collective, confined *in vivo* migration. We find that transient deformation and movement of the nucleus into the lead cell protrusion pries apart substrate cells to facilitate collective movement of cell clusters into spaces much smaller than even a single nucleus. Depletion of the *Drosophila* B-type lamin, Lam, compromises nuclear integrity, impedes border cell detachment, and hinders stabilization of a single lead protrusion. Together, these data indicate that cells can use nuclei as wedges to facilitate collective movement into confined space.

Summary

During confined, collective border cell migration, the lead cell nucleus functions as a wedge to pry apart substrate nurse cells. Although both A- and B- type lamins are expressed, the B-type is essential while the A-type is dispensable.

Keywords: lamin, nucleus, collective cell migration, cell contact

Introduction

Collective cell migration is critical for development and wound healing, and promotes cancer metastasis (Rørth, 2009; Friedl and Gilmour, 2009). One challenge for collective groups moving *in vivo* is the difficulty of squeezing into small spaces between cells, for example during intravasation and extravasation (Stoletov et al., 2010; Wyckoff et al., 2000; Reymond et al., 2013), or through dense extracellular matrix (ECM). How groups of cells physically crawl into narrow paths and navigate complex tissue environments is not well understood.

The nucleus, typically the largest and stiffest organelle, can pose a physical barrier to movement in confined spaces (Calero-Cuenca et al., 2018; Friedl et al., 2011). A-type and B-type lamins are proteins that assemble into distinct intermediate filament networks underneath the nuclear envelope (NE), and are primary contributors to nuclear mechanics (Hetzer, 2010; Davidson and Lammerding, 2014; Wintner et al., 2020; Lammerding et al., 2004). Higher expression of lamins, particularly A-type lamins, leads to increased nuclear stiffness (Swift et al., 2013; Ferrera et al., 2014). A-type lamin tends to be expressed at higher levels in stiff tissues while B-type expression is higher during development and in soft tissues such as the brain (Swift et al., 2013; Hutchison, 2014). Mouse embryonic fibroblasts, cancer cell lines, mesenchymal stem cells, and hematopoietic cells depleted of A-type lamins have more deformable nuclei and migrate faster through narrow channels or ECM *in vitro* (Rowat et al., 2013; Davidson et al., 2014; Harada et al., 2014; Shin et al., 2013), so nuclear stiffness can impede confined migration. However, other *in vitro* studies report that lamin A/C depletion reduces the ability of cells to move in confinement (Lee et al., 2021; Lomakin et al., 2020). How lamins contribute to confined migration through different *in vivo* environments is not well understood.

There are multiple models for how nuclear mechanics promote confined migration. In HeLa and primary progenitor zebrafish cells, nuclei sense physical compression by unfolding indentations in the nuclear envelope and triggering actomyosin contractions, which promote escape from the confinement (Lomakin et al., 2020; Venturini et al., 2020). Alternatively, the nuclear piston model initially reported in primary human fibroblasts (Petrie et al., 2014) and later observed in confined, mesenchymal stem cells (Lee et al., 2021) proposes that hydrostatic pressure builds up in confined cells, activating mechanosensitive ion channels that open and cause swelling and large bleb-like protrusions (Lee et al., 2021). In leukocytes, nuclei near the front of cells act as a mechanical gauge to find the path of least resistance (Renkawitz et al., 2019). A key open question is how nuclei sense, respond, and contribute to the migration of cell collectives *in vivo*.

Here, we use the border cell cluster in the *Drosophila* ovary as a model to study how nuclei change shape during and contribute to collective, confined, *in vivo* cell migration. We show that nuclei rapidly deform as cell clusters move in between tightly apposed nurse cells. Lead cell nuclei undergo the most significant shape changes, elongating as they extend into forward-directed protrusions, and then recovering elastically. Nuclear movement correlates with protrusion expansion. We further show that perturbations in nuclear structure impede migration. While both A- and B-type lamins are expressed, only the B-type lamin, Lam, is required to maintain nuclear integrity and to promote border cell migration, particularly during the onset of migration. Lam-depleted cells

extend transient forward protrusions that do not expand properly, as well as ectopic protrusions, ultimately resulting in uncoordinated movement. We propose that the nucleus functions as a wedge, which facilitates lead cell protrusion enlargement, stability, and thus coordinated movement of cell clusters into spaces that are initially much smaller than even a single nucleus. The lead cell nucleus also absorbs the brunt of forces, while the passenger polar cells are protected from nuclear deformations.

Results

To study the role of nuclei in collective cell migration, we used the well-established model of border cell migration in the *Drosophila* egg chamber. At stage 9, the border cell cluster delaminates from a layer of epithelial cells and squeezes in between germline cells, termed nurse cells, to reach the oocyte by stage 10 (Fig 1A-C). Border cells consist of a pair of inner, nonmotile polar cells and 4-6 outer, motile cells (Fig 1B). Typically, one outer border cell extends a large protrusion toward the oocyte and leads the cluster, though the leader can change over time. Lead border cells extend and retract protrusions, probing for chemoattractants and available space. The border cells select the central path between the nurse cells because it contains slightly larger spaces (Dai et al., 2020) (Fig. 1D); however even the largest spaces are much smaller than the cluster.

To assess the relative sizes and dynamics of the clusters, cells, nuclei and available spaces, we acquired time series images at delamination. We labeled extracellular spaces (junctures) with fluorescent 10 kDa dextrans (Fig. 1D), nuclei with a dsRED-tagged nuclear localization signal (NLS), border cells with a GFP-tagged actin-binding domain of moesin (Fig. 1D). The junctures that clusters initially moved into during delamination averaged 1.5 microns in diameter, which was 3 fold narrower than a single border cell nucleus (Fig. 1E-F). As border cells delaminated the leading protrusion widened, significantly expanding the juncture (Fig. 1F-H, S1A, Movie S1). These data suggest that leading protrusion pries apart nurse cells before nuclear translocation.

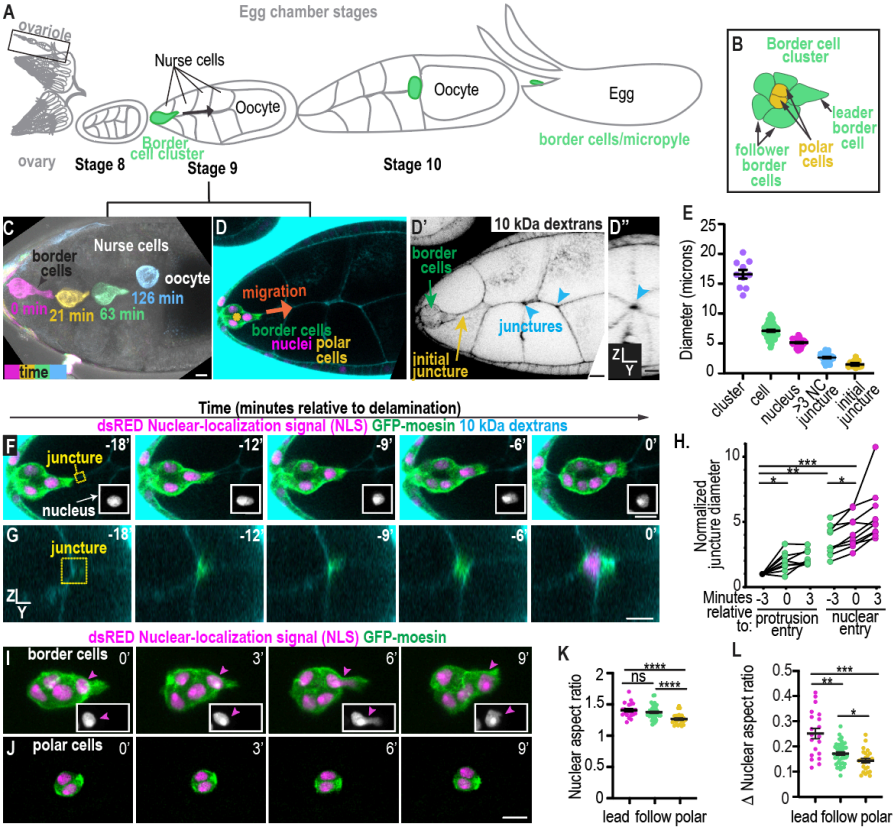

Fig. 1. Leader cells extend protrusions and transiently deform nuclei during the onset of border cell migration. A. Overview of the *Drosophila* ovary, ovariole, and egg chamber at different stages. B. Illustration of the border cells (green) and polar cells (purple). C. A max projection of images from a timelapse of a stage 9 egg chamber to show the border cell cluster movement over time. The egg chamber is shown with Differential Interference Contrast (DIC) and border cells expressing GFP-moesin are labeled with a different color for each timepoint. D. A stage 9 egg chamber expressing fruitlessGal4;UAS-GFP-moesin (border cells);UAS-dsRED.Nuclear localization signal (NLS) (nuclei) and incubated with 10 kDa dextran-Alexa647 to label junctures. D'- D'' show the inverted fluorescent image of the 10 kDa dextrans in both XY and YZ views to show possible paths for border cells to migrate on. Arrowheads mark central extracellular spaces which the border cells select to migrate in. Scale bar: 10 μm E. Plot showing individual diameters for indicated features. Average +/- standard error of the mean (SEM) are the center and error bars respectively. F-G. XY and YZ images of border cells and junctures from a timelapse series labeled with the indicated markers. Yellow box marks the same juncture shown in F and G. White box in F shows the leading cell's nucleus in greyscale. H. Plot showing juncture width relative to time of protrusion entry (green) and nuclear entry (magenta). A mixed effects model (REML) followed by a Tukey's multiple comparison test was performed for statistics. I-J. Example images from time lapse series of border cell nuclei (I) or polar cell nuclei (J) labeled with UAS-dsRED.NLS expressed by c306Gal4(I) or UpdGal4(J). Magenta arrowheads label the lead cell's nucleus. K-L Plots show the average nuclear aspect ratio (K) and average change in nuclear aspect ratio (L) for each cell type (dots) and average of all cells +/- SEM (bars) An ANOVA followed by Tukey post-hoc was performed. Scale bars: 10 μm.

The lead cell nucleus elongated as it moved into the protrusion (Fig. 1F, S1A) and then recovered a rounder shape as the protrusion widened (Fig. 1F, S1A-B), so nuclear shape was variable as nuclei transiently elongated into protrusions (Fig. 1F, S1B, Movie S1). The width of the juncture expanded to over 5 fold as the nucleus moved in (Fig. 1F-H). Thus, the leading cell nucleus transiently deforms as it moves, and its translocation correlates with further expansion of the spaces between substrate nurse cells.

Lead cell nuclei tended to constrict and elongate when entering the base of the protrusion (Fig. 1F,I, Fig. S1C, Movies S2-S3), This deformation occurred within a minute (Fig. S1C, Movies S2-S3), unlike the hours-long process of nuclear deformation reported in cells moving in plastic channels *in vitro* (Davidson et al., 2014). Lead cell nuclei changed shape the most, follower cells less so and inner, nonmotile polar cells had the lowest and least variable nuclear aspect ratio (Fig. 1I-L, Movies S3-S4). These data indicate nuclear dynamics vary based on position and/or cell type, and the lead cell nucleus experiences the most nuclear deformation during border cell migration.

To test if transient changes in nuclear shape occurred spontaneously or due to forces resulting from migration, we measured nuclear shapes in immobile border cells expressing a dominant negative form of the small GTPase Rac (RacN17). RacN17-expressing cells lack lead protrusions

and completely fail to move (Murphy and Montell, 1996). RacN17-expressing border cells had similar average nuclear aspect ratios but significantly lower variation in nuclear shape compared to control border cell nuclei (Fig. S1 D-H). Thus, outer border cell nuclei, particularly when leading the cluster, undergo transient shape changes as they migrate, whereas inner cells are protected.

A and B-type lamins form independent intermediate filament networks that confer mechanical support to the nuclear envelope (Wintner et al., 2020; Davidson and Lammerding, 2014; Xie et al., 2016). The *Drosophila* genome encodes one A-type lamin called *LamC* and one B-type lamin named *Lam* (Bossie and Sanders, 1993; Lenz-Böhme et al., 1997) (Fig. 2A). We found that both Lam and LamC antibodies stained the periphery of border cell nuclei, and protein levels were diminished in cells expressing the corresponding RNAi (Fig. 2B-E). Expressing two UAS-RNAi lines targeting separate regions of the Lam gene with a Gal4(c306Gal4) that drives expression in border and polar cells caused migration defects whereas LamC RNAi did not (Fig. 2F-L). Gal4 is more active at 29°C than at lower temperatures. When we incubated Lam RNAi-expressing flies at 29 ºC for 1 day, we observed variable knockdown, and the clusters with the most effective knockdown exhibited more severe migration defects (Fig. S2A-B). For a more robust expression of Gal4, we incubated Lam RNAi flies for 3 days at 29ºC, and found 82% of clusters expressing Lam RNAi line 107419, and 72% of clusters expressing Lam RNAi line 45635 showed incomplete migration at stage 10. In both lines, half of

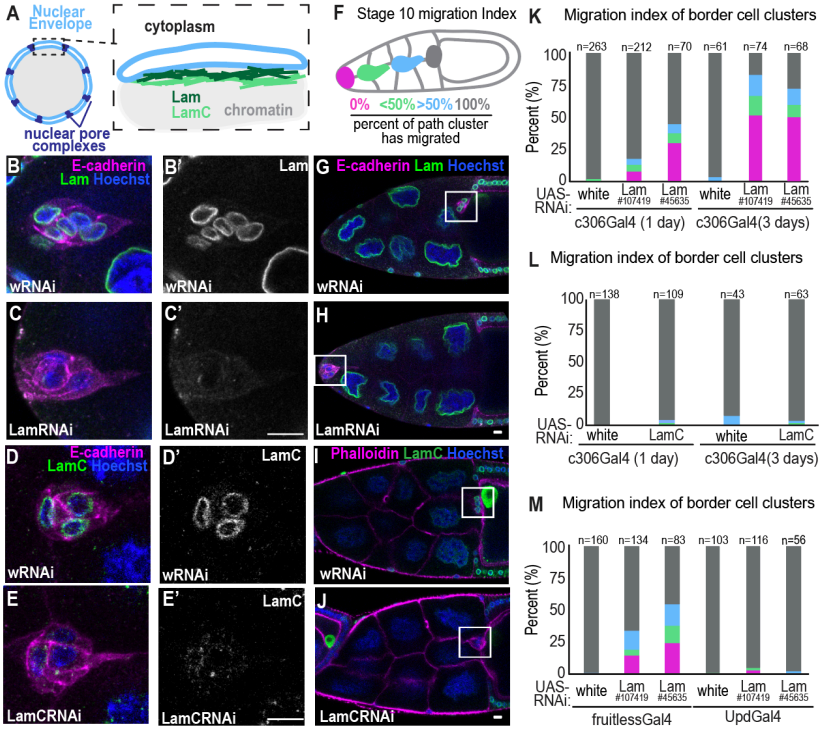

Fig. 2. B-type lamins promote border cell migration. A. Schematic of the nuclear envelope and the two *Drosophila* lamin proteins, Lam and LamC. B-E. Images of fixed border cell clusters stained with Lam (B-C) and LamC (D-E). Scale bar:10 microns. F. Schematic of migration index parameters. G-J. Images of fixed stage 10 egg chambers for the indicated conditions. The oocyte is always shown on the right and the white box marks the border cell cluster. K-M Plots showing migration indexes for indicated conditions. n=number of egg chambers.

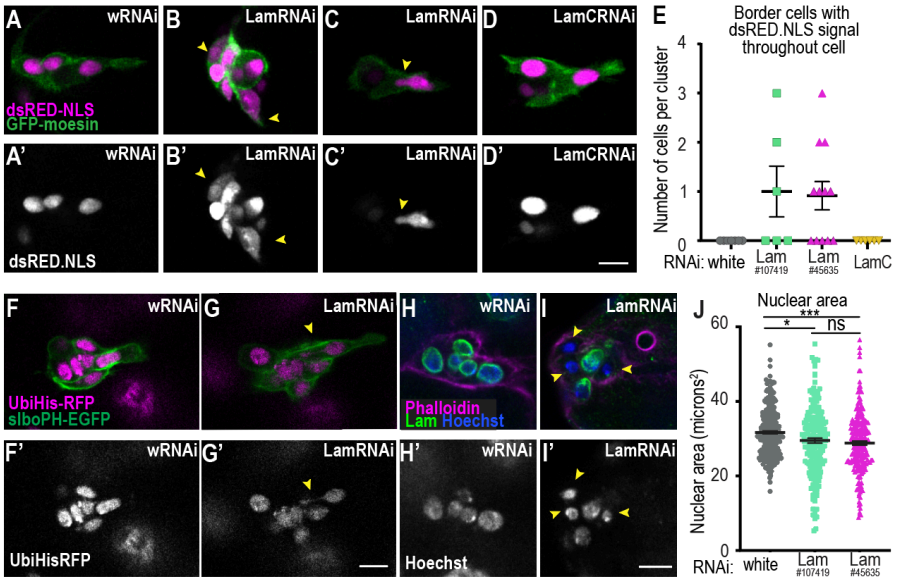

Fig. 3. B-type lamins are required for nuclear structure. A-D. Images of border cells from time lapse series in stage 9 egg chambers with the indicated markers and conditions. E. Plot measuring the average +/- SEM number of cells in a border cell cluster with dsRED.NLS throughout the cell. F-G. Images of border cells from time lapse series with the indicated markers and conditions. Yellow arrowhead marks rearward nuclear herniation. H-I Images of fixed border cell clusters stained with indicated markers for wRNAi (H) and LamRNAi (I) border cells. J. Measurements of nuclear area with each individual nucleus value shown as dots and bars representing mean +/- SEM. Statistical test: Kruskal Wallis test. Scale bars: 10 μm.

border cells failed to delaminate (Fig. 2K). Those Lam-depleted clusters that delaminated migrated at similar speeds to control clusters (Fig. S2C), indicating that B-type lamin is particularly important for delamination.

To test if Lam is required in the outer border cells or polar cells we crossed UAS-Lam RNAi lines to fruitlessGal4, which is expressed in border but not polar cells, and UpdGal4, which is expressed in polar but not border cells. LamRNAi expressed with fruitlessGal4 but not with UpdGal4 caused incomplete migration at stage 10 (Fig. 2M). We conclude the *Drosophila* B-type lamin is required in the outer, motile border cells.

Depletion of either A-type or B-type lamin disrupts the nuclear envelope permeability barrier in cultured cells (Vargas et al., 2012). To test how Lam and LamC KD affects border cell nuclei, we performed fixed and live imaging to assess nuclear structure and dynamics. We monitored nuclei with dsRED.NLS, which is retained in the nucleus when the nuclear permeability barrier is intact. Control and LamC depleted nuclei retained dsRED in the nuclear interior in all nuclei observed. By contrast, some Lam-depleted nuclei lost the permeability barrier and exhibited dsRED.NLS throughout the cell (Fig. 3A-

E). Live imaging revealed that Lam-depleted nuclei in leading cells produced herniations in the direction opposite to migration, whereas neither LamC-depleted nor control nuclei exhibited such herniations (Fig. 3A-D, F-G). Lam-depleted nuclei were also smaller than controls (Fig. 3H-J). We conclude that Lam is required to maintain nuclear integrity, shape, and size in border cells while LamC is less critical in this context.

Border cell fate specification, cluster formation and delamination require the activity of multiple transcription factors and their downstream targets. Lamins are required for chromatin organization and gene expression, in addition to their mechanical roles, so we tested the effect of Lam RNAi on border cell fate, cluster formation, and expression of genes required for delamination. Lam-depleted border cells still formed clusters that had similar numbers of cells as controls and rounded up (Fig. S3A). Further, Lam-depleted cells showed normal F-actin, E-cadherin and Singed (*Drosophila* Fascin) expression (Fig. S3B-D). STAT activation, which is essential for border cell specification, was increased in Lam-depleted cells at stage 8 (Fig. S3E-H). Notch activity, which is required for border cell delamination, was similar to controls (Fig. S3I-J). We conclude that Lam is not required for border cell specification or for known regulators of delamination.

The data suggested that nuclear structural defects might impede the ability of Lam-depleted cells to move into confined space during border cell delamination. To determine how Lam depletion affected the dynamics of border cells during delamination and migration, we monitored border cell membranes with time-lapse microscopy of stage 9 egg chambers. LamRNAi-expressing clusters produced thin, ectopic protrusions while controls maintained a lead cell protrusion (Fig. 4A-B, Movies S5-S6). Lam-depleted clusters sometimes moved between anterior follicle cells and germ cells instead of taking their normal central path, but did not progress and began to move back towards the anterior of the egg chamber (Fig. 4B and Movie S6).

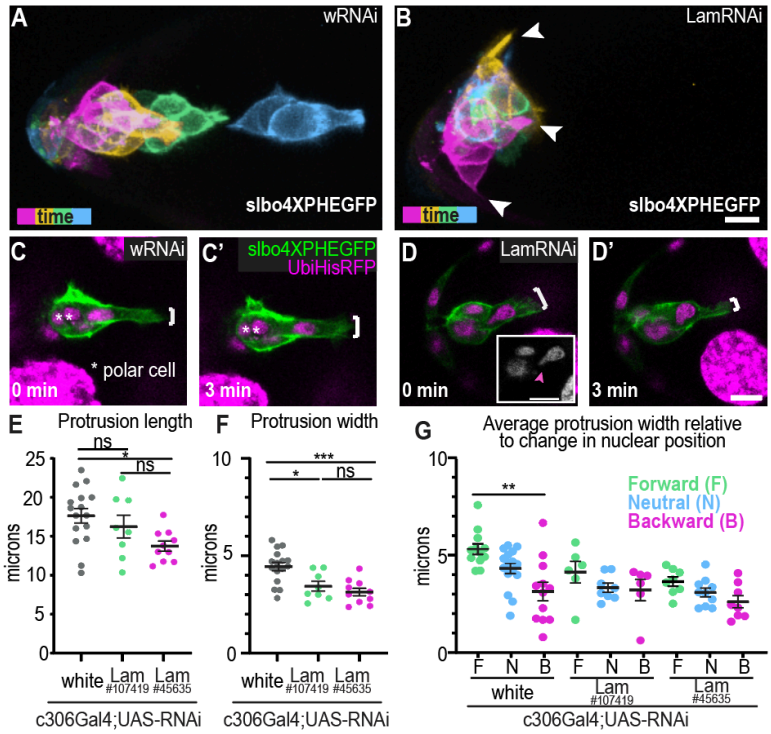

Fig. 4. B-type lamins promote the expansion of a single protrusion. A-B Maximum projections of time frames from time lapse series of stage 9 egg chambers expressing slbo4xPHEGFP to mark border cell membranes in control (wRNAi, A) and Lam-depleted border cells (LamRNAi, B). Time points relative to the start of imaging: magenta=0 minutes, yellow=33 minutes, green=54 minutes, blue=108 minutes. Arrowheads mark protrusions. C-D Single z-slice images from time lapse series of migrating control border cells (wRNAi, C) or Lam-depleted border cells that delaminate but fail to expand the protrusion (D). White bars show protrusion width. E-G. Plots showing average +/- SEM and individual values (dots) of the average length (E) and width of protrusions (F,G) for the indicated conditions. G shows protrusion width after nuclear movement for each RNAi line. An ANOVA with Tukey post-hoc was performed for each plot. Scale bars: 10 μm.

We next assessed how nuclear dynamics related to protrusion dynamics. Leading cell nuclei in controls moved into protrusions, which corresponded with a widening of the protrusion neck (Fig 4C, Movie S7). In lamin-depleted clusters, nuclei extended forward, but couldn't stably remain in the protrusion neck, leading to protrusion narrowing (Fig. 4D, Movie S8). On average, protrusions were shorter and thinner in LamRNAi -expressing cells compared to controls (Fig. 4E-F). In control leading cells, nuclear movement forward into the protrusion was associated with protrusion widening, while backward movement correlated with protrusion narrowing (Fig. 4G). In contrast, there was no major difference in protrusion width with nuclear movement in Lam-depleted cells. These data suggest that a nucleus extending into the protrusion neck may help stabilize and/or expand the protrusion, and protrusion expansion is impaired when nuclei have a weaker lamina. We conclude that Lam is required to maintain and expand the leading protrusion, prevent ectopic protrusions, and move through the center of the egg chamber.

To test whether a second perturbation of nuclear structure would cause similar effects, we altered the expression of another nuclear envelope protein, Lamin B receptor (LBR) (Wagner et al., 2004). LBR is an inner nuclear membrane protein that binds lamins and chromatin, and overexpression of LBR is responsible for the multilobed nuclei that allow neutrophils to squeeze into and out of blood vessels and tissues (Hoffmann et al., 2002). Overexpression of LBR also causes irregular nuclear morphology in *Drosophila* embryos (Hampoelz et al., 2016). In control and LBR-overexpressing border cells, LBR localized at the nuclear periphery (Fig. 5A-B). Nuclei overexpressing LBR became elongated (Fig. 5B-E). To test if LBR overexpression disrupted migration in border cells or polar cells, we crossed UAS-LBR and a control (UAS-LacZ) to fruitlessGal4 and UpdGal4. Overexpression of LBR with fruitlessGal4 but not UpdGal4 caused significant migration defects, indicating LBR OE only disrupts migration through functions in motile border cells (Fig. 5F). Thus, LBR overexpression disrupts nuclear shape and impedes border cell movement between nurse cells, supporting that nuclear structure is required for this confined migration.

Discussion

Here we present an *in vivo* study of nuclei in cell clusters migrating into tissue spaces that are smaller than even a single nucleus. *In vivo,* cells migrate through diverse terrains: they can move on basement membranes or through ECM gels; but they can also squeeze between cells or in spaces between ECM and cells (Mishra et al., 2019a; Rørth, 2009; Yamada and Sixt, 2019). An important difference between cell movement through matrix versus between cells is that migrating cells can secrete proteases to open larger spaces in matrix (Wolf et al., 2013; Yamada and Sixt, 2019; Wolf et al., 2007). However, cells migrating between other cells, for

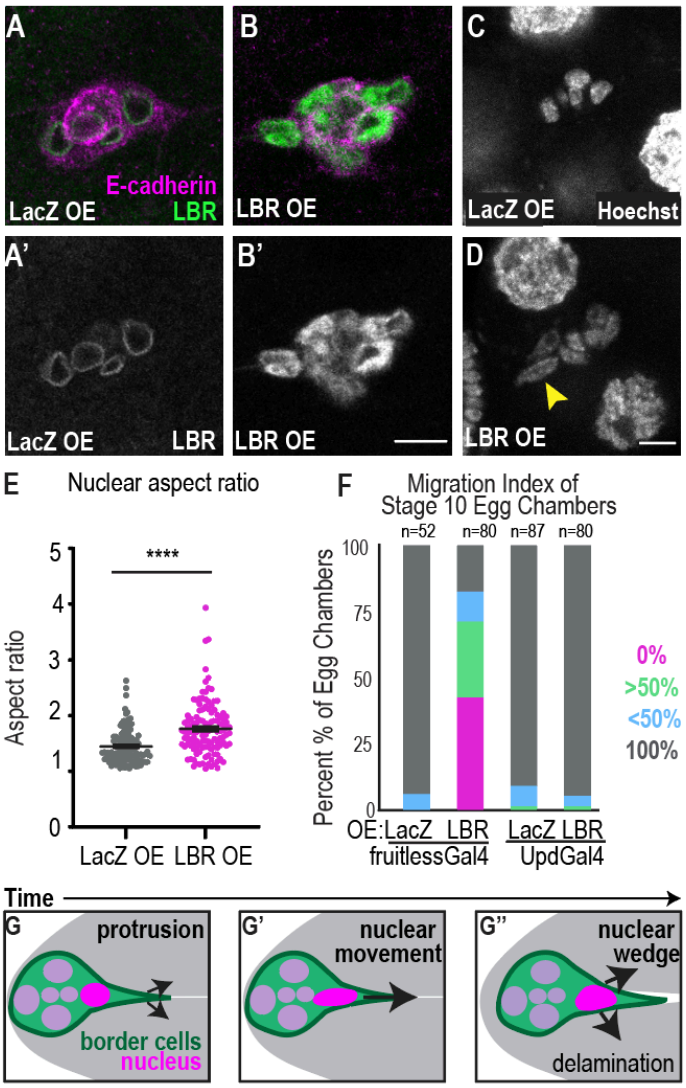

Fig. 5. Lamin B receptor overexpression disrupts border cell migration and nuclear structure. A-B. Images of fixed border cells from stage 9 egg chambers stained for Lamin B receptor (LBR) with LacZ overexpressed (A) LBR overexpressed (B) with c306Gal4 for 1 day at 29 ºC. C-D. Images of Hoechst staining of stage 9 egg chambers overexpressing LacZ(C) or LBR(D) kept at 29 ºC for 1 day. Scale bars: 10 μm.E. Plots measuring nuclear shape in nuclear aspect ratio from Hoechst channel of fixed border cell. Each dot represents an individual nucleus and middle and error bars represent the mean +/- SEM. A Mann-Whitney test was used for statistical testing. F. Plot of migration indexes of staged egg chambers in the noted conditions. n=number of egg chambers counted. G. Nuclear wedge model in collective border cell migration.

example during transendothelial migration or during embryonic development, do not have the option to degrade the substrate. Instead, they must pry the substrate cells apart. Here, we report the dynamics of nuclei during border cell migration and discover a novel role for the nucleus in this collective, confined, *in vivo* cell migration. We propose a nuclear wedge model (Fig. 5G), whereby F-actin-rich protrusions begin to pry nurse cells apart but then the nucleus has to move in and provide mechanical support to the protrusion to prevent its collapse and allow it to enlarge.

Lead cell protrusions serve multiple functions in migrating border cells. They are sensory structures that probe for chemoattractants and available space (Dai et al., 2020). The data presented here suggest an additional function for the lead cell protrusion – physical enlargement of the available space in front of the cluster. The idea that the protrusion can physically expand space has been observed in hydrogels *in vitro* (Lee et al., 2021) and is supported by our *in vivo* study. Our data also suggest that movement of the nucleus into the base of the protrusion prevents its collapse and thereby facilitates protrusion growth and enlargement, which is essential for the cluster to advance into the tiny spaces between nurse cells (Fig. 5G). Since disrupting nuclear integrity by depleting Lam impedes border cell migration, these data suggest that the nucleus promotes this confined *in vivo* migration.

Depletion of Lam results in border cells with thin and ectopic protrusions (Fig. 4), indicating that the B-type lamin at the nuclear envelope promotes enlargement and stabilization of the lead cell protrusion. Previous work shows that mechanical feedback from the dominant lead protrusion inhibits side and rear protrusion (Cai et al., 2014; Mishra et al., 2019b). Thus, without maintenance of a single protrusion towards the center of the egg chamber in Lam-depleted cells, overall cluster front/back polarization fails to stabilize, side protrusions extend, and clusters either fail to migrate or attempt to take an abnormal trajectory (Fig. 4). These data also show that the B-type lamin is required to maintain nuclear size and mechanical integrity. The observation that Lam-depleted leading cells exhibit rearward nuclear herniations suggests that Lam normally counteracts rearward forces at protrusion necks, to prevent collapse and facilitate growth. While we have not ruled out the possibility that lamin's role in gene expression could also contribute to migration, we have detected no change in cell fate or differentiation or in their ability to generate dynamic protrusions in Lam knockdown border cells.

Leading border cell nuclei deform as they move into the protrusion, somewhat reminiscent of nuclei in single cells migrating through narrow *in vitro* channels, (Davidson et al., 2014; Krause et al., 2019). Yet border cell nuclear deformations occur on a much faster time scale (<1 min compared to hours). After deforming, the nuclei recover a round shape and this elastic rebound corresponds with widening of the protrusion. These differences from *in vitro* studies may be due to the different stiffnesses of the *in vivo* vs *in vitro* environments, since egg chambers are estimated to be 100 fold softer than the plastic (PDMS) used to fabricate microchannels (Johnston et al., 2014; Lamb et al., 2021).

Nuclear translocation in between nurse cell junctures corresponds with expansion of the path, consistent with the idea that the nucleus functions as a wedge to pry nurse cells apart. This is distinct from two other mechanisms by which nuclei promote motility into confined space. In the "nuclear piston" model (Petrie et al., 2014; Lee et al., 2021), ion channels induce protrusion expansion and in the "nuclear ruler" model, they increase actomyosin contractility at the cortex (Lomakin et al., 2020; Venturini et al., 2020). Protrusion expansion through osmotic pressure induced by the nuclear piston has been reported to occur over several hours *in vitro* (Lee et al., 2021), so this is unlikely to be the mechanism by which border cell nuclei rapidly deform. The nuclear ruler model proposes that when nuclei are compressed sufficiently, unfolding of the nuclear envelope can activate cortical myosin within minutes through a lipid signaling mechanism. However in this case the nuclei remain stretched, while border cell nuclei exhibit elasticity and rapidly recover a more round shape. It will be of interest to investigate which, if any, of these mechanisms coexist in cells and under what conditions the different mechanisms contribute to confined motility. Purely mechanical processes

operate on faster time scales than chemical reactions and thus seem like the most likely explanation for the changes reported here in border cell nuclei.

We also show that follower cells and inner polar cells undergo less nuclear deformation than the leading cell, suggesting that one advantage of collective movement is that cells behind the leaders are protected from nuclear deformation. Since severe deformations can result in nuclear rupture and DNA damage (Irianto et al., 2017; Denais et al., 2016; Raab et al., 2016), such protection could be physiologically significant for cells moving collectively during wound healing and tumor metastasis.

Materials and Methods

Drosophila genetics

Drosophila stocks used in this study are described in Table 1. Flies were maintained in cornmeal-yeast food. To combine Gal4s with different UAS-lines, 5-7 virgin females were crossed to 2-3 males in the presence or absence of the temperature-sensitive repressor Gal80TS. For lines without Gal80TS, crosses were maintained at 25 °C and flies were transferred into new vials every 2-3 days. For Gal4 lines with Gal80TS, crosses were kept at 18 °C, and progeny were supplemented with yeast and incubated at 29 °C for 3 days prior to dissection (Fig. 5F). For FlpOUT experiments to generate mosaic clones (Fig. S3I-J), flies were heat shocked 1 hour at 37 °C, restored to 25 °C for four hours, heat shocked again for 1 hour, and fattened for 3 days at 29 °C. Crosses with c306Gal4 were fattened for both 1 day and 3 days 29 °C prior to dissection for stage 10 migration indices (Fig. 2K-L), but 1 day incubation at 29 °C was performed before all other experiments. For all other dissections, flies were supplemented with yeast at 29 °C for 1 day prior.

Table 1. *Drosophila* Stocks.

Stock description and genotype	Source
c306Gal4	Lab stock
FruitlessGal4	Lab stock
UpdGal4	Lab Stock
hsFLP, AyGal4; UAS-GFP	Lab Stock Generated from BDSC #4411 and #1929
UAS-LamRNAi	VDRC, #107419
UAS-LamRNAi	VDRC, #45635
UAS-whiteRNAi/CyO	Lab stock
UAS-LacZ	BDSC, #3956
UAS-LBR	BDSC, #43417
UAS-RacN17	Lab stock
UAS-LamCRNAi	BDSC, #31621
UAS-Stinger	BDSC, #84277
10XSTATGFP (STAT92e)	Lab stock
UAS-dsRed.NLS; UAS-moesin-GFP	Lab stock
Notch responsive element(NRE)-Red Reporter	Lab stock
c306Gal4; UbiHisRFP, slbo4xPH-EGFP	Lab Stock

Immunostaining and Fixed Imaging

Ovaries were dissected in Schneider's media (Thermo Fisher Scientific) supplemented with 20% heat-inactivated Fetal Bovine Serum (Sigma-Aldrich) and 1x antimycotic/antibiotic (VWR) and adjusted to a pH of 6.85-6.95. Ovaries were then fixed in 4% paraformaldehyde in 1X Phosphate-buffered saline (PBS) for 15 minutes. Ovarioles were washed 3x 10 minutes with 1X PBS +0.4% triton (PBST) and incubated in primary antibodies overnight at 4 °C. Antibodies used include: Lam (1:10, DHSB ADL84.12), E-cadherin (1:15 DHSB DCAD2), LamC (1:20, DHSB LC28.26), singed (1:20, DHSB, sn 7c), and Lamin B receptor (1:200 gift from Dr. Georg Krohne). The following day, ovaries were washed with 1X PBST followed by 3x10 minutes washes in 1X PBST. Then, ovaries were incubated with secondary antibodies (Goat anti-Rat IgG (H+L) Cross-Adsorbed Secondary Antibody, Alexa Fluor 647 and 568, Invitrogen, Goat anti-Mouse IgG (H+L) Cross-Adsorbed Secondary Antibody, Alexa Fluor 488 and 568, Invitrogen), phalloidin-647 (1:500), and Hoechst (1:500) for 1 hour at room temperature. Ovaries were washed with 1XPBST followed by 3x10 minutes washes in 1X PBST. After the last wash, ovaries are suspended in vectashield (H-1000, Vector Laboratories) and incubated overnight at 4 °C before mounting onto slides.

Slides were imaged on a Zeiss LSM780 confocal microscope with a 40× 1.1 N.A. 0.62mm long working distance water objective.

Live Imaging

Ovarioles were dissected from ovaries in live imaging media (Schneider's media (Thermo Fisher Scientific) supplemented with 20% heat-inactivated Fetal Bovine Serum (Sigma-Aldrich) and 1x antimycotic/antibiotic (VWR) with a pH of 6.85-6.95) and resuspended in live imaging media with 0.4 mg/mL insulin and 1% agarose and immediately mounted for imaging. Stage 9 egg chambers were imaged on an inverted Zeiss LSM800 confocal microscope fitted with a Plan-Apochromat 40X, 1.2 NA multi-immersion objective with the collar set for water immersion at 3, 2 minutes or 20 seconds time intervals as specified in figures and movies.

For imaging with dextrans to mark extracellular spaces, fluorescent dextrans were added to the media prior to mounting (100 µg/ml; Dextran Alexa 647 10,000 MW; Thermo Fisher Scientific; D22914).

Image analysis

Diameter measurements

For each movie, the diameters of clusters, cells, nuclei, and junctures in the central path were measured prior to delamination for the first timeframe (Fig. 1E). The outline of each cell, nucleus, and the entire cluster were manually traced from fluorescent markers in ImageJ (GFP-moesin for border cells, and dsRED.NLS for nuclei and dextran-Alexa647 junctures).

Protrusion shape analysis

The time of delamination (Fig. 1F, S1A-B) was scored as the full detachment of all border cells from the anterior of the egg chamber and set as time=0 for the measurements and all time points were set relative to delamination=0 minutes. UAS-GFP-moesin actin binding domain was expressed in border cells by fruitlessGal4 (Fig. 1F, S1A-B) or slbo4XPHEGFP (Fig. 4) was used to mark the border cells boundaries. To measure protrusion length, a line that was parallel to the long axis of the

egg chamber was drawn from the polar cell boundary to the protrusion tip. To measure protrusion width, lines were manually drawn across the protrusion at the widest position perpendicular to the long axis of the egg chamber and measured in Image J for each time point.

Nuclear movement and shape analysis

To measure nuclear position in the protruding cells (Fig. 4G), a line was manually drawn from the back of the nucleus to the nearest polar cell membrane marked with slbo4XPHE-GFP for each time point. The change in nuclear position was measured as the change in length of the line between two time points and divided by the time interval. Only the largest protrusion was scored for each timepoint if there were multiple protrusions, and analysis was only performed in protruding cells. To set a threshold for forward, neutral or backward nuclear movement, the average and standard deviation were calculated for the data set, and forward movement was defined as >1 standard deviation (SD) greater than the mean, neutral was defined as within 1 SD from the mean, and backward was defined as more than 1 SD lower than the mean.

To measure the nuclear aspect ratio (regardless of egg chamber orientation) from time-lapse series for comparison of leader, follower, and polar cell nuclei (Fig. 1K-L) as well as the control versus RacN17 nuclei (Fig. S1G-H), the central z-slice of the channel with UAS.dsRED.NLS in each nucleus was cropped from each time point to prevent overlap of nuclei during semiautomated analysis. Nuclei were segmented into binary images using a custom Matlab code (available upon request), and shape parameters were measured over time using the analyze particle tools in ImageJ. We manually verified if the segmentation worked properly and whether the nucleus was in view of not. If the automated analysis did not properly segment the nucleus in a time point, a manual trace was performed. Samples were blinded throughout the analysis. All timeframes were included unless the nucleus went out of focus during the imaging session. The average nuclear aspect ratio was automatically generated in ImageJ measurements. The change in nuclear aspect ratio was calculated by taking the absolute value between two aspect ratios of adjacent time points. Statistical testing was performed in R using an ANOVA blocked by movie variation with Tukey post-hoc analysis for nuclear shape analysis.

To measure the lead cell's nuclear aspect ratio relative to the migration axis lines (Fig S1A-B), lines were manually drawn across the center of the nucleus marked with dsRED.NLS parallel and perpendicular to the long axis of the egg chamber. The aspect ratio was calculated by dividing the parallel nuclear diameter by the perpendicular nuclear diameter.

For fixed imaging analysis of nuclear shape, the Hoecsht signal in fixed border cells proved difficult to segment automatically. Therefore, each nucleus in a border cell cluster was traced manually in Image J by using the Hoechst signal to mark the nucleus in stage 9 egg chambers. All border cells' nuclei were included unless Hoechst staining did not allow distinguishing of a nucleus from background or if a nucleus was out of focus. ImageJ measurements were used to calculate area and aspect ratio of traces of nuclei in fixed images.

Border cell migration indexes

To measure border cell migration defects, all stage 10 egg chambers were identified by onset of centripetal cell migration, and the border cell cluster was detected with E-cadherin or phalloidin staining. The position of the border cell cluster was manually scored based on positions (0%: still attached, <50% migrated relative to distance between anterior and oocyte boundary, >50% migrated relative to anterior:oocyte, and 100%: at oocyte boundary). Then, the position of the cluster was recorded for each stage egg chamber. RNAi and overexpression experiments were performed at least 3 times independently with 3 independent genetic crosses, and with the control line (UAS-whiteRNAi or UAS-LacZ) crossed in parallel.

Migration speed

To measure the average speed of each border cell cluster, the z-slices from time-lapse series were max-projected. Then, the egg chamber was aligned over timepoints to correct for drift using the StackReg plugin in ImageJ. The manual tracking plugin in ImageJ was used to track border cell cluster position over time after delamination.

Lamin staining and border cell number

In stage 10 egg chambers, the number of border cells was manually counted using Hoechst and border cell markers (E-cadherin or Phalloidin). These cell number counts were limited to 30 micron z-sections, which usually covered the entire cluster. Lamin depletion was categorized as "none" (complete rim around the Hoechst signal), "partial" (incomplete rim around Hoechst), or "full" (no detectable lamin at the nuclear rim). The percent of border cells with full, partial, or no knockdown were divided by the total number of border cells in the cluster. The averages from each LamRNAi line are shown in Fig. S2A. Then, the averages were calculated for completed migration or incomplete migration in the LamRNAi (line #45635) (Fig. S2B).

STAT reporter quantification

To measure STAT activity in Stage 8 egg chambers, we crossed c306Gal4/Y; 10XSTATGFP (STAT92e)/CyO to UAS-LamRNAi or UAS-wRNAi lines. We performed immunostaining and imaged the anterior of stage 8 egg chambers. All egg chambers were imaged using the same conditions. For each egg chamber, we drew a small region of interest in each of the 2 cells adjacent to the polar cells in ImageJ and acquired the average fluorescent intensity and then subtracted a box in the nurse cells as background. Then, averages were normalized to the average of the UAS-wRNAi control to show the relative change in the fluorescence of the STAT reporter from the control.

Notch Responsive element quantification

To measure Notch activity, we generated a fly co-expressing UAS-LamRNAi (line #107419) or UAS-wRNAi with a Notch Responsive Element-Red Reporter (NRE-RR) (Zacharioudaki and Bray, 2014), and crossed these flies to a hsFlpAyGal4;UAS-GFP line. We heat shocked progeny as described above to generate clones. Only clusters with GFP+ clones were used for analysis. For measurements of NRE-RR fluorescent intensity, a box overlaying the nucleus was drawn in the center of each border cell and subtracted the average fluorescent intensity of a box drawn in the nurse cells (background). For each cluster, the average fluorescence intensity of the GFP+ clones was divided by the average fluorescent intensity of the GFP- clones in the same cluster.

Statistical analysis and data presentation

Prior to statistical analysis, experimental replicates were performed at least three times with separate genetic crosses. All undamaged samples were included for analysis. Nuclear shape analyses from live imaging were blinded. All other measurements were not blinded but performed in a systematic manner to minimize bias. Data were analyzed for normality using a Shapiro-Wilk normality test in Prism. A parametric test was performed for normally distributed data. If data did not pass the normality test, a nonparametric test was performed in prism. Statistical tests used and sample size are reported in figure legends. *$p<0.05$ **$p<0.01$ ***$p<0.001$ ****$p<0.0001$. Data points, middle bars and error bars are specified in the legends. Fluorescence images were acquired and processed exactly the same for control and experimental conditions. Figure legends include additional information on data representation for each specific experiment.

End Matter

Acknowledgments

We would like to thank the Bloomington Drosophila Stock Center, the Vienna Drosophila Resource Center (VDRC) for the Drosophila stocks. We would like to thank Georg Krohne for the Lamin B receptor antibody. We would like to thank Carinna Tran and Jim Mondo for their technical assistance and the members of the Montell lab for their feedback on this work. This work was supported by NIH grant R01GM073164 to D.J.M. and by the American Cancer Society Postdoctoral Fellowship (PF-22-091-01-MM) to L.P.

Author Contributions

L.P. and D.J.M. designed research, L.P. performed research, L.P. analyzed data; and L.P and D.J.M wrote the paper.

References

Bossie, C.A., and M.M. Sanders. 1993. A cDNA from Drosophila melanogaster encodes a lamin C-like intermediate filament protein. *J. Cell Sci.* 104 (Pt 4):1263–1272. doi:10.1242/jcs.104.4.1263.

Cai, D., S.-C. Chen, M. Prasad, L. He, X. Wang, V. Choesmel-Cadamuro, J.K. Sawyer, G. Danuser, and D.J. Montell. 2014. Mechanical feedback through E-cadherin promotes direction sensing during collective cell migration. *Cell*. 157:1146–1159. doi:10.1016/j.cell.2014.03.045.

Calero-Cuenca, F.J., C.S. Janota, and E.R. Gomes. 2018. Dealing with the nucleus during cell migration. *Curr. Opin. Cell Biol.* 50:35–41. doi:10.1016/j.ceb.2018.01.014.

Dai, W., X. Guo, Y. Cao, J.A. Mondo, J.P. Campanale, B.J. Montell, H. Burrous, S. Streichan, N. Gov, W.-J. Rappel, and D.J. Montell. 2020. Tissue topography steers migrating Drosophila border cells. *Science*. 370:987–990. doi:10.1126/science.aaz4741.

Davidson, P.M., C. Denais, M.C. Bakshi, and J. Lammerding. 2014. Nuclear deformability constitutes a rate-limiting step during cell migration in 3-D environments. *Cell. Mol. Bioeng.* 7:293–306. doi:10.1007/s12195-014-0342-y.

Davidson, P.M., and J. Lammerding. 2014. Broken nuclei--lamins, nuclear mechanics, and disease. *Trends Cell Biol.* 24:247–256. doi:10.1016/j.tcb.2013.11.004.

Denais, C.M., R.M. Gilbert, P. Isermann, A.L. McGregor, M. te Lindert, B. Weigelin, P.M. Davidson, P. Friedl, K. Wolf, and J. Lammerding. 2016. Nuclear envelope rupture and repair during cancer cell migration. *Science*. 352:353–358. doi:10.1126/science.aad7297.

Ferrera, D., C. Canale, R. Marotta, N. Mazzaro, M. Gritti, M. Mazzanti, S. Capellari, P. Cortelli, and L. Gasparini. 2014. Lamin B1 overexpression increases nuclear rigidity in autosomal dominant leukodystrophy fibroblasts. *FASEB J.* 28:3906–3918. doi:10.1096/fj.13-247635.

Friedl, P., and D. Gilmour. 2009. Collective cell migration in morphogenesis, regeneration and cancer. *Nat. Rev. Mol. Cell Biol.* 10:445–457. doi:10.1038/nrm2720.

Friedl, P., K. Wolf, and J. Lammerding. 2011. Nuclear mechanics during cell migration. *Curr. Opin. Cell Biol.* 23:55–64. doi:10.1016/j.ceb.2010.10.015.

Hampoelz, B., M.-T. Mackmull, P. Machado, P. Ronchi, K.H. Bui, N. Schieber, R. Santarella-Mellwig, A. Necakov, A. Andrés-Pons, J.M. Philippe, T. Lecuit, Y. Schwab, and M. Beck. 2016. Pre-assembled Nuclear Pores Insert into the Nuclear Envelope during Early Development. *Cell*. 166:664–678. doi:10.1016/j.cell.2016.06.015.

Harada, T., J. Swift, J. Irianto, J.-W. Shin, K.R. Spinler, A. Athirasala, R. Diegmiller, P.C.D.P. Dingal, I.L. Ivanovska, and D.E. Discher. 2014. Nuclear lamin stiffness is a barrier to 3D migration, but softness can limit survival. *J. Cell Biol.* 204:669–682. doi:10.1083/jcb.201308029.

Hetzer, M.W. 2010. The nuclear envelope. *Cold Spring Harb. Perspect. Biol.* 2:a000539. doi:10.1101/cshperspect.a000539.

Hoffmann, K., C.K. Dreger, A.L. Olins, D.E. Olins, L.D. Shultz, B. Lucke, H. Karl, R. Kaps, D. Müller, A. Vayá, J. Aznar, R.E. Ware, N. Sotelo Cruz, T.H. Lindner, H. Herrmann, A. Reis, and K. Sperling. 2002. Mutations in the gene encoding the lamin B receptor produce an altered nuclear morphology in granulocytes (Pelger-Huët anomaly). *Nat. Genet.* 31:410–414. doi:10.1038/ng925.

Hutchison, C.J. 2014. B-type lamins in health and disease. *Semin. Cell Dev. Biol.* 29:158–163. doi:10.1016/j.semcdb.2013.12.012.

Irianto, J., Y. Xia, C.R. Pfeifer, A. Athirasala, J. Ji, C. Alvey, M. Tewari, R.R. Bennett, S.M. Harding, A.J. Liu, R.A. Greenberg, and D.E. Discher. 2017. DNA Damage Follows Repair Factor Depletion and Portends Genome Variation in Cancer Cells after Pore Migration. *Curr. Biol.* 27:210–223. doi:10.1016/j.cub.2016.11.049.

Johnston, I.D., D.K. McCluskey, C.K.L. Tan, and M.C. Tracey. 2014. Mechanical characterization of bulk Sylgard 184 for microfluidics and microengineering. *J. Micromech. Microeng.* 24:035017. doi:10.1088/0960-1317/24/3/035017.

Krause, M., F.W. Yang, M. Te Lindert, P. Isermann, J. Schepens, R.J.A. Maas, C. Venkataraman, J. Lammerding, A. Madzvamuse, W. Hendriks, J. Te Riet, and K. Wolf. 2019. Cell migration through three-dimensional confining pores: speed accelerations by deformation and recoil of the nucleus. *Philos. Trans. R. Soc. Lond. B Biol. Sci.* 374:20180225. doi:10.1098/rstb.2018.0225.

Lamb, M.C., C.P. Kaluarachchi, T.I. Lansakara, S.Q. Mellentine, Y. Lan, A.V. Tivanski, and T.L. Tootle. 2021. Fascin limits Myosin activity within Drosophila border cells to control substrate stiffness and promote migration. *eLife*. 10. doi:10.7554/eLife.69836.

Lammerding, J., P.C. Schulze, T. Takahashi, S. Kozlov, T. Sullivan, R.D. Kamm, C.L. Stewart, and R.T. Lee. 2004. Lamin A/C deficiency causes defective nuclear mechanics and mechanotransduction. *J. Clin. Invest.* 113:370–378. doi:10.1172/JCI19670.

Lee, H.-P., F. Alisafaei, K. Adebawale, J. Chang, V.B. Shenoy, and O. Chaudhuri. 2021. The nuclear piston activates mechanosensitive ion channels to generate cell migration paths in confining microenvironments. *Sci. Adv.* 7. doi:10.1126/sciadv.abd4058.

Lenz-Böhme, B., J. Wismar, S. Fuchs, R. Reifegerste, E. Buchner, H. Betz, and B. Schmitt. 1997. Insertional mutation of the Drosophila nuclear lamin Dm0 gene results in defective nuclear envelopes, clustering of nuclear pore complexes, and accumulation of annulate lamellae. *J. Cell Biol.* 137:1001–1016. doi:10.1083/jcb.137.5.1001.

Lomakin, A.J., C.J. Cattin, D. Cuvelier, Z. Alraies, M. Molina, G.P.F. Nader, N. Srivastava, P.J. Sáez, J.M. Garcia-Arcos, I.Y. Zhitnyak, A. Bhargava, M.K. Driscoll, E.S. Welf, R. Fiolka, R.J. Petrie, N.S. De Silva, J.M. González-Granado, N. Manel, A.M. Lennon-Duménil, D.J. Müller, and M. Piel. 2020. The nucleus acts as a ruler tailoring cell responses to spatial constraints. *Science*. 370. doi:10.1126/science.aba2894.

Mishra, A.K., J.P. Campanale, J.A. Mondo, and D.J. Montell. 2019a. Cell interactions in collective cell migration. *Development*. 146. doi:10.1242/dev.172056.

Mishra, A.K., J.A. Mondo, J.P. Campanale, and D.J. Montell. 2019b. Coordination of protrusion dynamics within and between collectively migrating border cells by myosin II. *Mol. Biol. Cell*. 30:2490–2502. doi:10.1091/mbc.E19-02-0124.

Murphy, A.M., and D.J. Montell. 1996. Cell type-specific roles for Cdc42, Rac, and RhoL in Drosophila oogenesis. *J. Cell Biol.* 133:617–630. doi:10.1083/jcb.133.3.617.

Petrie, R.J., H. Koo, and K.M. Yamada. 2014. Generation of compartmentalized pressure by a nuclear piston governs cell motility in a 3D matrix. *Science*. 345:1062–1065. doi:10.1126/science.1256965.

Raab, M., M. Gentili, H. de Belly, H.R. Thiam, P. Vargas, A.J. Jimenez, F. Lautenschlaeger, R. Voituriez, A.M. Lennon-Duménil, N. Manel, and M. Piel. 2016. ESCRT III repairs nuclear envelope ruptures during cell migration to limit DNA damage and cell death. *Science*. 352:359–362. doi:10.1126/science.aad7611.

Renkawitz, J., A. Kopf, J. Stopp, I. de Vries, M.K. Driscoll, J. Merrin, R. Hauschild, E.S. Welf, G. Danuser, R. Fiolka, and M. Sixt. 2019. Nuclear positioning facilitates amoeboid migration along the path of least resistance. *Nature*. 568:546–550. doi:10.1038/s41586-019-1087-5.

Reymond, N., B.B. d'Água, and A.J. Ridley. 2013. Crossing the endothelial barrier during metastasis. *Nat. Rev. Cancer*. 13:858–870. doi:10.1038/nrc3628.

Rørth, P. 2009. Collective cell migration. *Annu. Rev. Cell Dev. Biol.* 25:407–429. doi:10.1146/annurev.cellbio.042308.113231.

Rowat, A.C., D.E. Jaalouk, M. Zwerger, W.L. Ung, I.A. Eydelnant, D.E. Olins, A.L. Olins, H. Herrmann, D.A. Weitz, and J. Lammerding. 2013. Nuclear envelope composition determines the ability of neutrophil-

type cells to passage through micron-scale constrictions. *J. Biol. Chem.* 288:8610–8618. doi:10.1074/jbc.M112.441535.

Shin, J.-W., K.R. Spinler, J. Swift, J.A. Chasis, N. Mohandas, and D.E. Discher. 2013. Lamins regulate cell trafficking and lineage maturation of adult human hematopoietic cells. *Proc Natl Acad Sci USA*. 110:18892–18897. doi:10.1073/pnas.1304996110.

Stoletov, K., H. Kato, E. Zardouzian, J. Kelber, J. Yang, S. Shattil, and R. Klemke. 2010. Visualizing extravasation dynamics of metastatic tumor cells. *J. Cell Sci.* 123:2332–2341. doi:10.1242/jcs.069443.

Swift, J., I.L. Ivanovska, A. Buxboim, T. Harada, P.C.D.P. Dingal, J. Pinter, J.D. Pajerowski, K.R. Spinler, J.-W. Shin, M. Tewari, F. Rehfeldt, D.W. Speicher, and D.E. Discher. 2013. Nuclear lamin-A scales with tissue stiffness and enhances matrix-directed differentiation. *Science*. 341:1240104. doi:10.1126/science.1240104.

Vargas, J.D., E.M. Hatch, D.J. Anderson, and M.W. Hetzer. 2012. Transient nuclear envelope rupturing during interphase in human cancer cells. *Nucleus*. 3:88–100. doi:10.4161/nucl.18954.

Venturini, V., F. Pezzano, F. Català Castro, H.-M. Häkkinen, S. Jiménez-Delgado, M. Colomer-Rosell, M. Marro, Q. Tolosa-Ramon, S. Paz-López, M.A. Valverde, J. Weghuber, P. Loza-Alvarez, M. Krieg, S. Wieser, and V. Ruprecht. 2020. The nucleus measures shape changes for cellular proprioception to control dynamic cell behavior. *Science*. 370. doi:10.1126/science.aba2644.

Wagner, N., D. Weber, S. Seitz, and G. Krohne. 2004. The lamin B receptor of Drosophila melanogaster. *J. Cell Sci.* 117:2015–2028. doi:10.1242/jcs.01052.

Wintner, O., N. Hirsch-Attas, M. Schlossberg, F. Brofman, R. Friedman, M. Kupervaser, D. Kitsberg, and A. Buxboim. 2020. A unified linear viscoelastic model of the cell nucleus defines the mechanical contributions of lamins and chromatin. *Adv Sci (Weinh)*. 7:1901222. doi:10.1002/advs.201901222.

Wolf, K., M. Te Lindert, M. Krause, S. Alexander, J. Te Riet, A.L. Willis, R.M. Hoffman, C.G. Figdor, S.J. Weiss, and P. Friedl. 2013. Physical limits of cell migration: control by ECM space and nuclear deformation and tuning by proteolysis and traction force. *J. Cell Biol.* 201:1069–1084. doi:10.1083/jcb.201210152.

Wolf, K., Y.I. Wu, Y. Liu, J. Geiger, E. Tam, C. Overall, M.S. Stack, and P. Friedl. 2007. Multi-step pericellular proteolysis controls the transition from individual to collective cancer cell invasion. *Nat. Cell Biol.* 9:893–904. doi:10.1038/ncb1616.

Wyckoff, J.B., J.G. Jones, J.S. Condeelis, and J.E. Segall. 2000. A critical step in metastasis: in vivo analysis of intravasation at the primary tumor. *Cancer Res.* 60:2504–2511.

Xie, W., A. Chojnowski, T. Boudier, J.S.Y. Lim, S. Ahmed, Z. Ser, C. Stewart, and B. Burke. 2016. A-type Lamins Form Distinct Filamentous Networks with Differential Nuclear Pore Complex Associations. *Curr. Biol.* 26:2651–2658. doi:10.1016/j.cub.2016.07.049.

Yamada, K.M., and M. Sixt. 2019. Mechanisms of 3D cell migration. *Nat. Rev. Mol. Cell Biol.* 20:738–752. doi:10.1038/s41580-019-0172-9.

Zacharioudaki, E., and S.J. Bray. 2014. Tools and methods for studying Notch signaling in Drosophila melanogaster. *Methods*. 68:173–182. doi:10.1016/j.ymeth.2014.03.029.

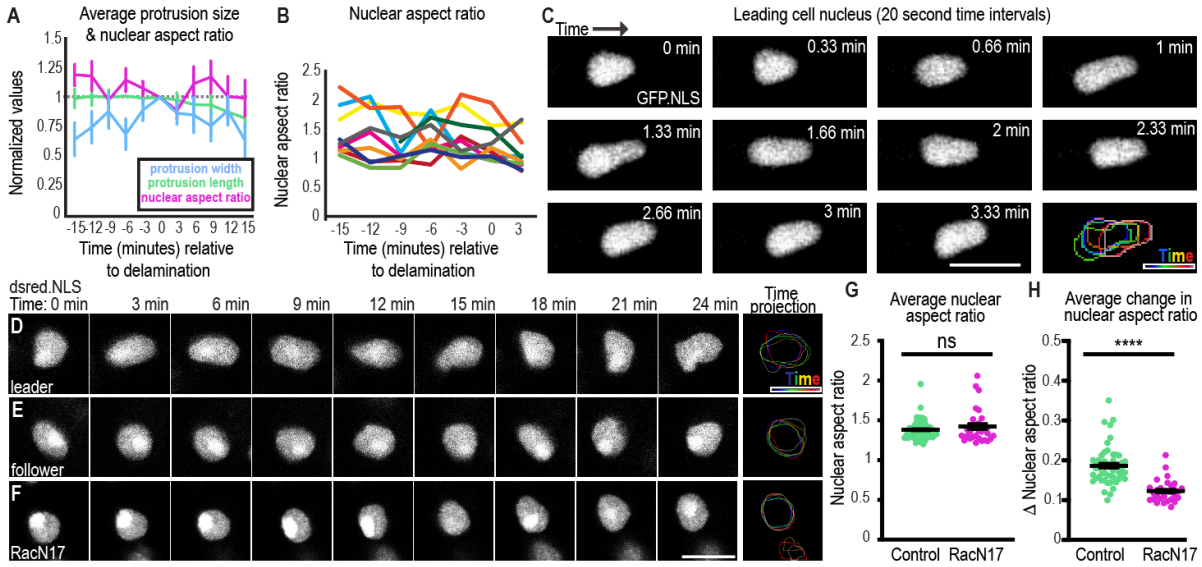

Fig. S1. Changes in nuclear shape occur rapidly in migrating border cell clusters. A. Plots of the average +/- SEM of each indicated parameter relative to the time of delamination. N=10 border cell clusters. B. Nuclear aspect ratio of each leading cell's nucleus aligned to the protrusion axis. C. Images from a timelapse series with the leading cell nucleus marked with GFP.NLS. Images were acquired every 20 seconds. Short time-interval movies were performed on at least 3 separate days/replicates. D-F. Example images of nuclei from time-lapse series of control leader, follower or RacN17 dominant negative expressing border cells. Right: projection of timepoints. G-H. Plots of the average (G) and average change (H) in nuclear aspect ratio. A Mann-Whitney test was used to test for statistical significance. Scale bars: 10 µm.

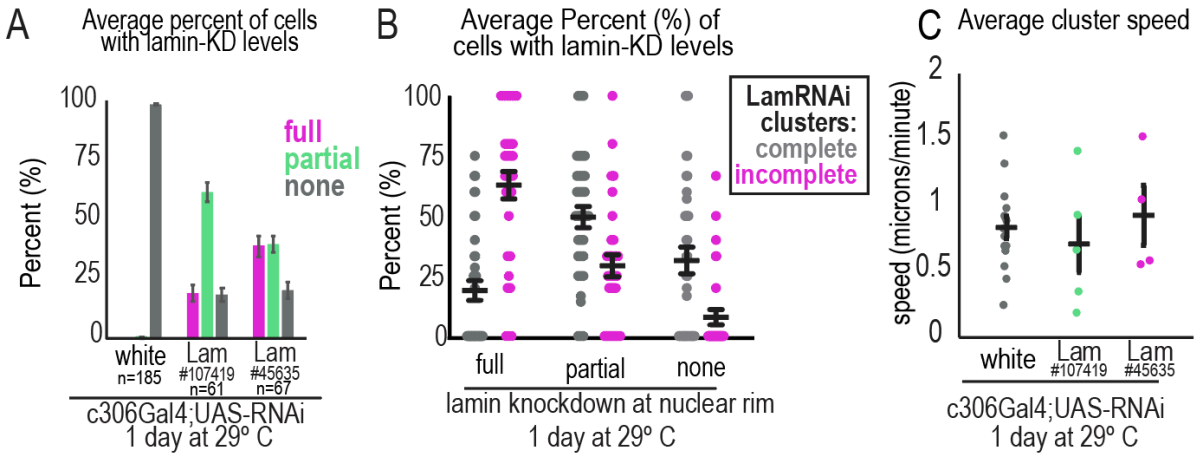

Fig. S2. Stronger depletion of lamins correlates with higher rates of migration defects. A. Plot showing the mean +/- SEM percentage of border cells with the indicated lamin depletion (full, partial or none). B. Plot showing the individual and average percent of cells with indicated knockdown (full, partial or none) for clusters that completed (gray) or did not complete (magenta) migration by stage 10. Analysis was performed on the LamRNAi line #45635. C. Average speed of delaminated clusters (dots) and the mean +/- SEM of each condition (black bars).

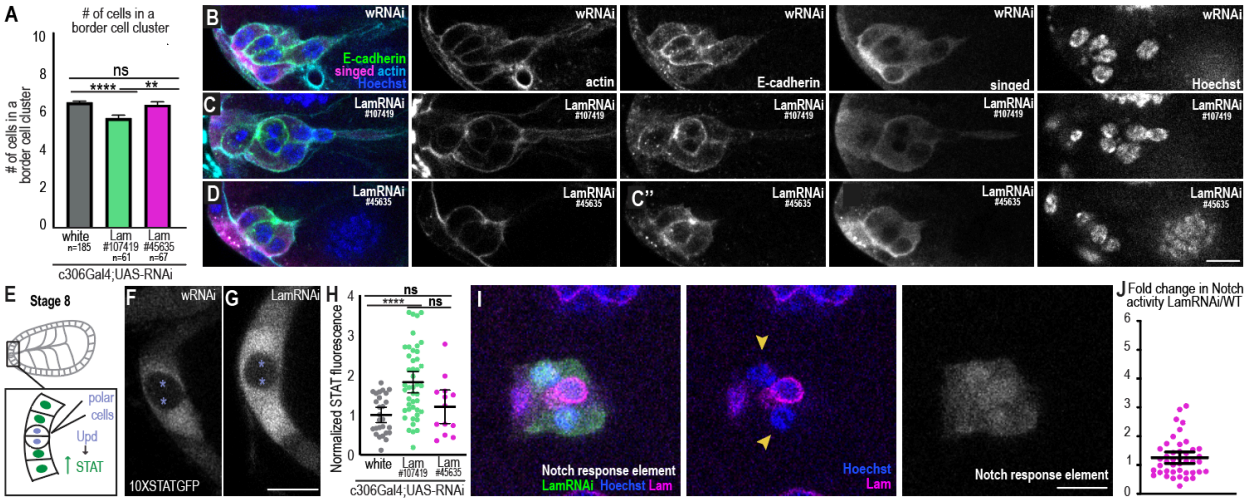

Fig. S3. Lam-depleted border cells specify and express key border cell genes. A. Average border cell number +/- SEM for indicated conditions. A Kruskal-Wallis test was performed to test for statistical significance. B-D Representative images of stage 9 border cells stained with the indicated markers in control (B) and LamRNAi (C-D). Left: merged images. Right: grayscale images of phalloidin, E-cadherin, singed, and Hoechst staining. E. Schematic of a stage 8 egg chamber and magnified view of polar cells and surrounding follicle cells. F-G. Confocal images of STAT activity reporter (10XSTATGFP) for indicated conditions. LamRNAi line shown: #107419. H. Plot showing individual (dots) and mean +/- SEM (bars) measures of STAT fluorescence normalized to the mean of the control E. Plot of mean +/- SEM border cell cluster number. A Kruskal-Wallis test was used for statistical testing. I. A border cell cluster expressing hsFlpAyGal4 UAS-GFP,LamRNAi clones and wildtype clones with the indicated markers. Left: Merge of channels. Middle: Images with only Lam and Hoechst staining to show loss of Lam staining in clones (arrows). Right: Greyscale image of notch responsive element-RFP. J. Plot showing the fluorescence intensity of the nuclear Notch responsive element relative to wildtype clones in the cluster. A Wilcoxon test was used to test for statistical upregulation, p=0.06, ns. Scale bars: 10 µm.

Supplemental Movies

Movies S1. Border cell clusters undergoing delamination. Single z-slices from a stage 9 egg chamber expressing fruitlessGal4; UAS-GFP-moesin actin-binding domain (border cells, green) UAS-dsRED.NLS (nuclei, magenta), and incubated with 10 kDa dextran-Alexa 647 (dextrans, cyan). Scale bar: 10 µm.

Movie S2. Border cell nuclei, particularly when leading, under rapid changes in nuclear shape. A max projection of a border cell cluster expressing GFP.Nuclear localization signal (NLS) at 20 second time intervals. Scale bar: 10 µm.

Movie S3. Border cell nuclei undergo dynamic shape changes. Border cell nuclei labeled with UAS-dsRED.NLS and clusters labeled with UAS.GFP-Moesin in lines expressing c306Gal4 (polar cells did not highly express dsRED.NLS). Scale bar: 10 µm.

Movie S4. Polar cells maintain nuclear shape during migration. Border cell clusters expressing UpdGal4;UAS-dsRED.NLS to label polar cell nuclei and UAS-GFP-moesin to label cells. Scale bar: 10 µm.

Movie S5. Control border cells stabilize a main protrusion to lead clusters. Movie of an egg chamber with controlRNAi border cell clusters (c306Gal4; UAS-wRNAi) expressing slbo4XPHEGFP to mark the border cells (green) and UbiHisRFP to mark all nuclei (magenta). Right panel shows slbo4XPHEGFP channel in grayscale. Scale bar: 10 µm.

Movie S6. Lam-depleted clusters form ectopic protrusions and have undirected movement. Movie of a timelapse of max-projected egg chamber with LamRNAi border cell clusters (c306Gal4; UAS-LamRNAi (#45635)) expressing slbo4XPHEGFP to mark the border cells (green) and UbiHisRFP to mark all nuclei (magenta). Right panel shows slbo4XPHEGFP in grayscale. Scale bar: 10 µm.

Movie S7. Nuclear stretching and movement corresponds with protrusion widening. Timelapse movie of controlRNAi border cells (c306Gal4; UAS-wRNAi) expressing slbo4XPHEGFP to mark the border cells (green) and UbiHisRFP to mark all nuclei (magenta). Right panel shows UbiHisRFP. Scale bar: 10 µm.

Movie S8. Lam-depleted cells do not stabilize protrusions. Timelapse movie of LamRNAi border cell clusters (c306Gal4; UAS-LamRNAi) expressing slbo4XPHEGFP to mark the border cells (green) and UbiHisRFP to mark all nuclei (magenta). Right panel shows the UbiHisRFP channel alone. Scale bar: 10 µm.